Int. J. Electrochem. Sci., 15 **(2020)** 9088 – 9107, doi: 10.20964/2020.09.04

International Journal of ELECTROCHEMICAL SCIENCE
www.electrochemsci.org

Synergistic Effect of Zinc/aluminium-layered Double Hydroxide-clopyralid Carbon Nanotubes Paste Electrode in the Electrochemical Response of Dopamine, Acetaminophen, and Bisphenol A

Nurashikin Abd Azis[1], *Illyas Md Isa*[1,2,*], *Norhayati Hashim*[1,2], *Mohamad Syahrizal Ahmad*[1,2], *Siti Nur Akmar Mohd Yazid*[1], *Mohamad Idris Saidin*[1,2], *Suyanta M.Si*[3], *Rahadian Zainul*[4], *Alizar Ulianas*[4], *Mawardi Mawardi*[4], *Siriboon Mukdasai*[5]

[1] Department of Chemistry, Faculty of Science and Mathematics, Universiti Pendidikan Sultan Idris, 35900 Tanjong Malim, Perak, Malaysia
[2] Nanotechnology Research Centre, Faculty of Science and Mathematics, Universiti Pendidikan Sultan Idris, 35900 Tanjong Malim, Perak, Malaysia
[3] Department of Chemistry Education, Faculty of Mathematics and Natural Science, Yogyakarta State University, Yogyakarta, Indonesia
[4]Fakultas Matematika dan Ilmu Pengetahuan Alam, Universitas Negeri Padang, Kota Padang, Sumatera Barat, Indonesia
[5] Department of Chemistry, Faculty of Science, Khon Kaen University, Khon Kaen 40002, Thailand
[*]E-mail: illyas@fsmt.upsi.edu.my

Received: 20 April 2020 / *Accepted:* 30 June 2020 / *Published:* 10 August 2020

A voltammetric sensor was developed using multiwalled carbon nanotubes (MWCNTs) paste electrode based zinc/aluminium-layered double hydroxide-clopyralid for simultaneous determination of dopamine (DA), acetaminophen (ACT), and bisphenol A (BPA). Several experimental conditions such as percent of modifier, pH of the solution, and square wave voltammetry parameters were optimized. The effective surface area of the electrodes was determined by chronocoulometry studies. The sensor demonstrated a linear plot of 7.0×10^{-6} – 5.0×10^{-4} M for DA, 3.0×10^{-5} – 5.0×10^{-4} M for ACT, and 3.0×10^{-6} – 5.0×10^{-4} M for BPA, with detection limit of 1.7×10^{-7} M, 1.8×10^{-7} M, and 1.4×10^{-7} M respectively. The interferences from 10 to 40-fold concentration of ascorbic acid, sodium salicylate, glucose, sucrose, glutamic acid, and captopril were negligible. The electrode also applicable for DA, ACT, and BPA determination in urine, pharmaceutical tablets, and plastic products samples with recoveries between 92.3 % and 109.7 %.

Keywords: Dopamine, Acetaminophen, Bisphenol A, Multiwalled carbon nanotubes, Square wave voltammetry, Nanocomposite

1. INTRODUCTION

Bisphenol A (BPA), is one of the endocrine disrupters that is capable of mimicking natural hormones [1]. BPA acts as a monomer in the manufacture of polycarbonate plastics such as food can lining, water containers, baby bottles, and medical devices. Human may regularly expose to trace amounts of BPA since this compound may leach upon heating. Exposure to BPA has been associated with adverse effects against reproductive, metabolic, and developmental of humans [2]. Furthermore, studies found that the exposure to BPA may increase anxiety-like behaviors and alters the level of neurotransmitter specifically dopamine [3,4].

Dopamine (DA) is a molecule that has basic centers, which consists of one amino and two phenolate sites [5]. It is exists in central nervous system and shows a critical role in controlling our motive and cognitive systems [6]. An abnormal levels of this neurotransmitter is generally known to be the cause of Parkinsonism [7] and Schizophrenia [8]. The suffering patients will undergo constant chronic pain due to motor function abnormalities which related to neurological problems. Thus, for some cases, painkillers such as acetaminophen was administered to the patients [9,10].

Acetaminophen (ACT) also known as paracetamol, was discovered in 1893 and has been widely used around the world as an analgesic and antipyretic. It is a worldwide known drug particularly due to its safe, effective, and available in various formulations [11]. The recommended maximum daily intake of ACT is 4 grams [12]. However, excessive intake of ACT may cause the accumulation of toxic metabolites which further lead to liver injury [13,14]. Thus, it is important in monitoring the level of ACT in human body. In connection of clinical and pharmacological importance BPA, DA, and ACT, a simple method for monitoring and determination of these compounds are required.

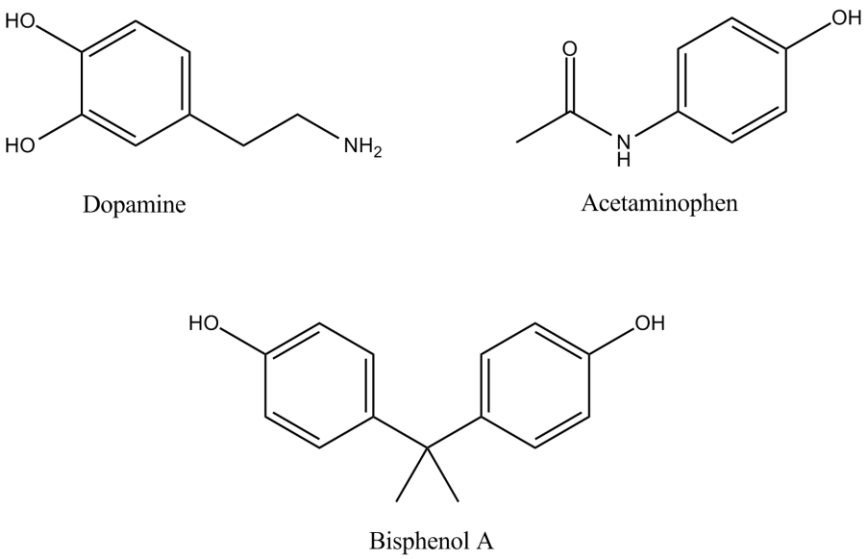

Figure 1. Chemical structure of dopamine, acetaminophen and bisphenol A.

Several analytical methods are applicable for the determination of BPA, DA, and ACT (Fig. 1) such as high performance liquid chromatography [15,16], Fourier transform infrared spectroscopy [17], solid phase extraction [18], chemiluminescence [19,20], and colorimetric [21,22]. Looking toward the necessity of providing sensitive, low cost, and portable monitoring for health, food and environmental issues, electrochemical sensor possessed these advantages. Generally, the performance of the electrochemical sensor depends on the material used as a working electrode. Due to poor performance exhibit by a bare electrode, some modifications have been proposed in order to develop a sensor with an excellent performance [23].

Carbon paste electrodes (CPEs) have gained much attention by researchers in the electrochemical sensor field due to their low-cost preparation. CPEs can be prepared with desired composition in order to fulfill certain electrode properties [23,24]. Multiwalled carbon nanotubes (MWCNTs) are much popular in CPEs production because they possess merits such as large surface area and stable against electromigration [25-28]. Apart from that, the application of nanomaterials in electrochemical field becoming popular to enhances the selectivity and sensitivity of the sensor. Recently, inorganic clays specifically layered double hydroxides (LDHs) have been extensively used electrode modifiers owing to their distinctive properties such as permanent positive charge, large surface area, low toxicity, thermally stable, and chemically inert [29,30]. They can be synthesized easily from available inorganic precursors [31]. One of the peculiar properties of LDH is that the interlayer anions can simply exchange with numerous organic and inorganic charged compounds. Moreover, LDH also can promote electron transfer between the analyte and electrode [32-34].

For instances, there were some reported applications of LDH in electrochemical determination of BPA, DA, and ACT such as Ni-Al-LDH/graphene hybrid/GCE [35], Ni-Al-LDH/carbon ionic liquid electrode [36], Mg-Al LDH/NHNPs/MWCNTs/GCE [37], Zn-LDH-*L*-phenylalanate/MWCNTs/CPE [38], exfoliated Ni_2Al-LDH/GCE [39], Mg-Al-CO_3-LDH/GCE [40], and Zn-Al ionic liquid-LDH/GCE [41]. Nevertheless, LDH has been used only for single determination of BPA, DA, or ACT. To the best of our studies, there is no report on simultaneous determination of BPA, DA, and ACT. Hence, this work is aimed to fabricate the MWCNT paste electrode modified by zinc/aluminium-layered double hydroxide-clopyralid nanocomposite (Zn/Al-LDH-CP) for the simultaneous determination of BPA, DA, and ACT.

2. EXPERIMENTAL

2.1. Reagents and chemicals

All analytical grade reagents were used without any purification. The MWCNT was from Timesnano (China) and the paraffin oil was from Merck (Germany). Stock solution of 1.0×10^{-2} M BPA, 1.0×10^{-2} M DA, and 1.0×10^{-2} M ACT were prepared by dissolving in 50 mL of deionized water and kept in a refrigerator at 4°C when not in used. Potassium phosphate buffer solution (PBS) as a supporting electrolyte was prepared by mixing the stock solution of 0.1 M K_2HPO_4 and 0.1 M KH_2PO_4.

2.2. Apparatus

Voltammetric and electrochemical impedance spectroscopy (EIS) analysis were performed using a Potentiostat Series-G750 and Potentiostat Ref 3000 (Gamry, USA), respectively. An electrochemical cell comprising of Ag/AgCl, platinum wire and modified MWCNT paste electrode as a reference electrode, counter electrode and working electrode, respectively. The surface morphology of Zn/Al-LDH-CP/MWCNT was observed using field emission scanning electron microscopy (FESEM), model SU8020 UHR (Hitachi, Japan) and transmission electron microscope (TEM), model JEOL-2000EX (Japan). The pH of the solution was measured by using Thermo Scientific Orion 2-Star Benchtop pH Meter (USA).

2.3. Synthesis of zinc/aluminium-layered double hydroxide-clopyralid nanocomposite (Zn/Al-LDH-CP)

Zn/Al-LDH-CP was synthesized by using $Zn(NO_3)_2$ and $Al(NO_3)_3$ as precursors via co-precipitation method [31]. The precursors were dissolved in 250 mL of deionized water with the molar ratio R = 3. A few drops of sodium hydroxide were added to achieve the desired pH (7.5 ± 0.05). The mixture was then added with 100 mL of 0.1 M clopyralid (CP) solution and stirred under a nitrogen atmosphere. The resulting suspension was aged in oil bath shaker at 70°C for 24 hours and then centrifuged. The precipitate was thoroughly washed with deionized water and dried in oven at 60°C. The dried product of Zn/Al-LDH-CP was finely ground and kept in a bottle.

2.4. Preparation of electrodes

Different ratios of MWCNTs (100, 95, 90, 85 % w/w) and Zn/Al-LDH-CP (0, 5, 10, 15 % w/w) were mixed via hand mixing in a mortar and pestle. A few drops of paraffin oil were added to the mixture. The homogenized paste was tightly pressed into the Teflon tube (i.d. 2.0 mm, long 3.0 cm). One end of the tube was inserted with a copper wire to establish the electrical contact, while the other end of the tube was polished on a filter paper just before used.

2.5. Real sample analysis

Urine, pharmaceutical tablets, and baby teether were used as real samples for DA, ACT, and BPA, respectively. The urine samples were obtained from two healthy people and diluted 100 times in deionized water [42]. The pharmaceutical tablets containing 500 mg and 120 mg of paracetamol were powdered and weighted to the corresponding 1000 mg L^{-1} amounts of paracetamol. The samples were dissolved in deionized water and sonicated [43]. The baby teether was soaked in 20.0 mL ethanol and heated for 4 hours at 50.0°C. The mixture was filtered and the solvent obtained was completely evaporated. 3.0 mL of ethanol was added to the residue and diluted in 50.0 mL PBS [44].

3. RESULTS AND DISCUSSION

3.1. Surface morphology studies of Zn/Al-LDH-CP

The SEM image of Zn/Al-LDH-CP and the TEM image of Zn/Al-LDH-CP/MWCNT are shown in Figs. 2A and 2B, respectively. The surface morphology studies reveal that Zn/Al-LDH-CP has irregular structure and appears as flake-like shape [31]. The mixture of Zn/Al-LDH-CP/MWCNT observed under TEM showed the transparent tube represents MWCNTs, while the opaque part represents Zn/Al-LDH-CP. It was quite clear from this image that Zn/Al-LDH-CP possesses a layered morphology and displays the successful of amalgamation of MWCNTs and the modifier [45].

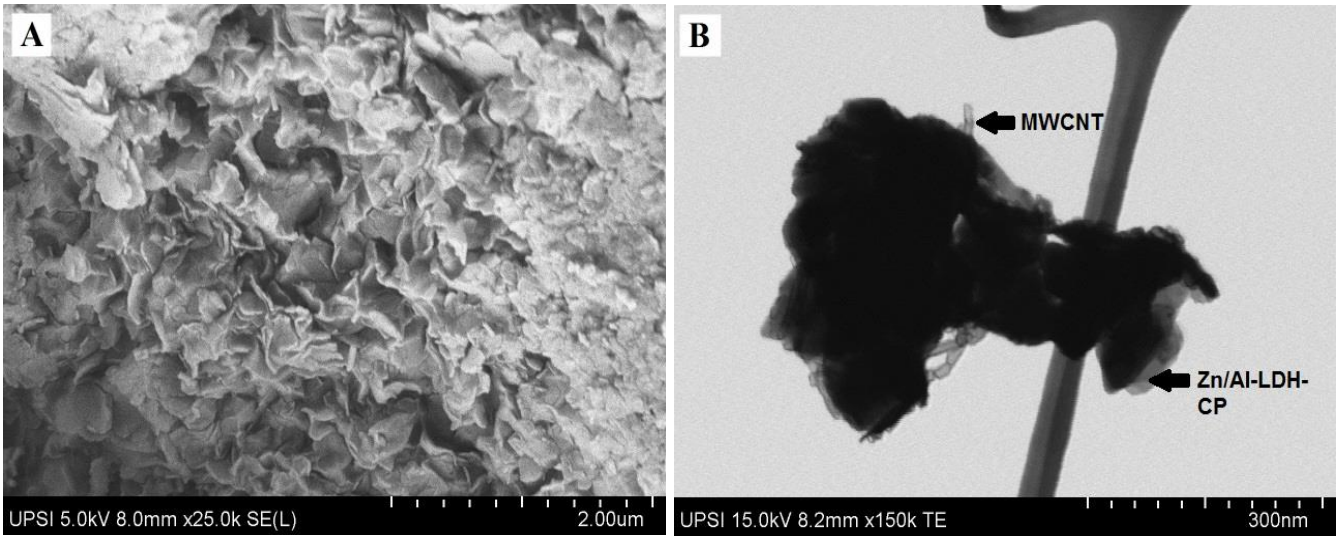

Figure 2. (A) Image of Zn/Al-LDH-CP observed under SEM and (B) Image of Zn/Al-LDH-CP/MWCNT mixture observed under TEM.

3.2. Characterization of MWCNTs and Zn/Al-LDH-CP/MWCNTs

The performance of MWCNTs and Zn/Al-LDH-CP/MWCNTs paste electrodes towards 4.0×10^{-3} M $K_4Fe(CN)_6$ containing 0.1 M KCl were evaluated using cyclic voltammetry (CV) to study the electron transfer nature of sensing materials. As illustrated in Fig. 3, Zn/Al-LDH-CP/MWCNTs paste electrode (curve b) exhibited higher redox currents than MWCNT paste electrode (curve a). The anodic peak current (I_{pa}) obtained for MWCNTs paste electrode was 6.011 μA and the cathodic peak current (I_{pc}) was 3.698 μA. Meanwhile, the redox peak current of Zn/Al-LDH-CP/MWCNTs paste electrode was increased to I_{pa} = 10.70 μA and I_{pc} = 8.916 μA. Moreover, peak-to-peak separation (ΔE_p) of Zn/Al-LDH-CP/MWCNTs paste electrode also decreased from 0.3497 V to 0.3178 V, which could be ascribed to the successful implementation of sensing materials to the MWCNTs paste electrode by increasing the electron transfer rate and the conductivity of the electrode.

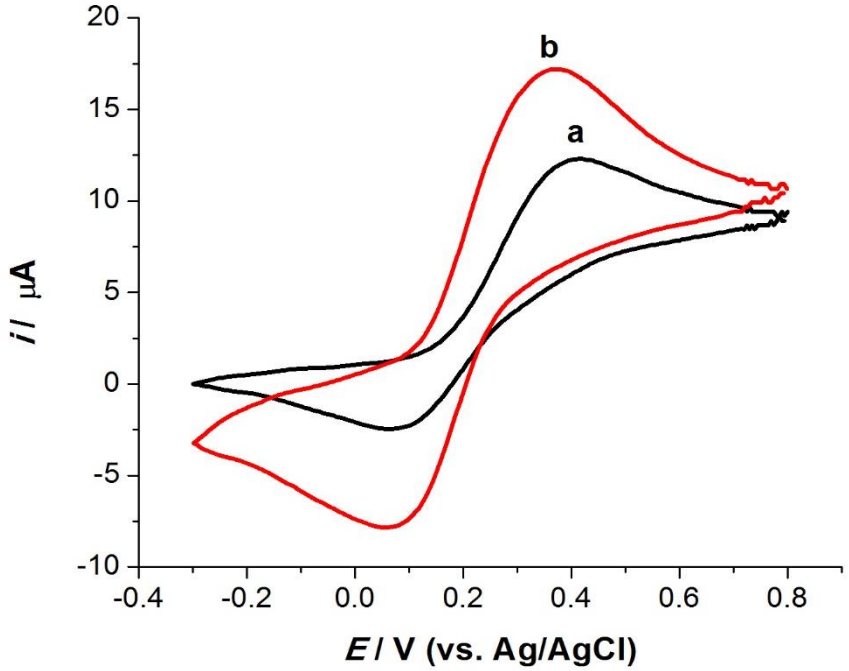

Figure 3. Cyclic voltammograms of (a) MWCNT paste electrode and (b) Zn/Al-LDH-CP/MWCNT paste electrodes in 4.0×10^{-3} M $K_4Fe(CN)_6$ containing 0.1 M KCl. Scan rate 100 mVs^{-1}.

EIS analysis was conducted for further studies on the electrode surface. Fig. 4 displays the Nyquist plots of EIS which consist of two portions. Generally, the semicircle part represents the electron transfer-limited process, while their diameter corresponds to the charge transfer resistance (R_{ct}) at the electrode surface. The linear part refers to the diffusion process. The semicircle of the Zn/Al-LDH-CP/MWCNTs paste electrode (curve b) was approximately two times smaller than MWCNTs paste electrode (curve a), suggested that the modification of the MWCNTs paste electrode by using Zn/Al-LDH-CP has led to the decreasing in impedance and further facilitate the electrochemical reaction on electrode surface [46]. In addition, the electron transfer apparent rate constant (k_{app}) for both electrodes were calculated according to the following equation:

$$k_{app} = \frac{RT}{F^2 R_{ct} AC}$$

Where R is the gas constant (8.314 J mol^{-1} K^{-1}), T is the absolute temperature of the system (298 K), and F is the Faraday constant (96485 C mol^{-1}), A is the estimated area of the electrode and C is the concentration of the $K_4Fe(CN)_6$ solution. The k_{app} values calculated for MWCNTs paste electrode and Zn/Al-LDH-CP/MWCNTs paste electrode were 1.44×10^{-4} cm s^{-1} and 2.72×10^{-4} cm s^{-1}, respectively. The Zn/Al-LDH-CP/MWCNTs paste electrode exhibited high k_{app} and low R_{ct} values, indicated a faster electron transfer process on the interface, which could be accelerated by the presence of Zn/Al-LDH-CP.

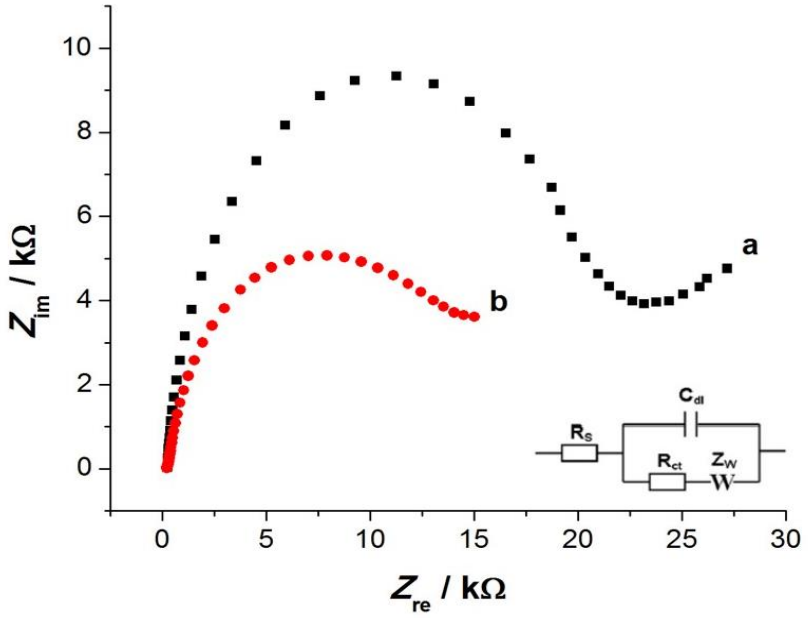

Figure 4. Nyquist plot of (a) MWCNT paste electrodes, and (b) Zn/Al-LDH-CP/MWCNT paste electrodes in 4.0×10^{-3} M $K_4Fe(CN)_6$.

3.3. Electrochemical behaviors of DA, ACT, and BPA

The electrochemical behaviors of 1.0×10^{-4} M of DA, ACT, and BPA at a MWCNTs and Zn/Al-LDH-CP/MWCNTs paste electrode were studied using square wave voltammetry technique. Fig. 5 shows that the Zn/Al-LDH-CP/MWCNTs paste electrode displayed a better peak current and resolution compare to MWCNTs paste electrode. These results indicate that the alteration of MWCNTs paste electrode with Zn/Al-LDH-CP has significantly improve the response in a simultaneously determination of DA, ACT, and BPA.

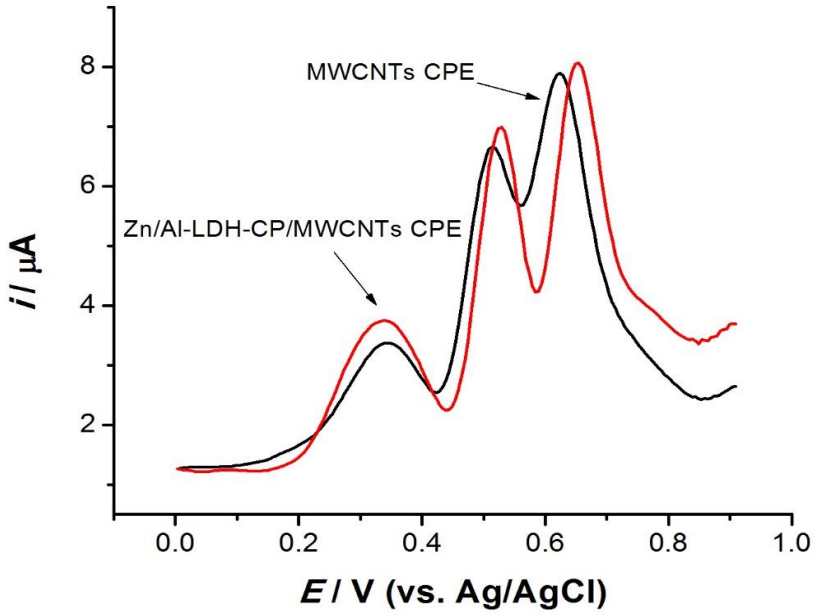

Figure 5. SWV of MWCNT and Zn/Al-LDH-CP/MWCNT paste electrodes in 1×10^{-4} M DA, ACT, and BPA solution.

3.4. Optimization of the experimental conditions

3.4.1. Percentage of modifiers

The performance of the electrode towards the different percentage of modifiers was studied in 1.0×10^{-4} M of DA, ACT, and BPA solution at pH 7.0 by using SWV. As shown in Fig. 6, the MWCNTs paste electrode with 5 % of Zn/Al-LDH-CP exhibited a high current response compare to the bare electrode. Further increased in the amount of modifier cause the current response to decrease possibly due to the formation of a thick film at the electrode surface which limits the mass transport of electrons and reduce the conductivity of the electrode. Hence, the modified MWCNTs paste electrode with 5 % of Zn/Al-LDH-CP was used for the following studies.

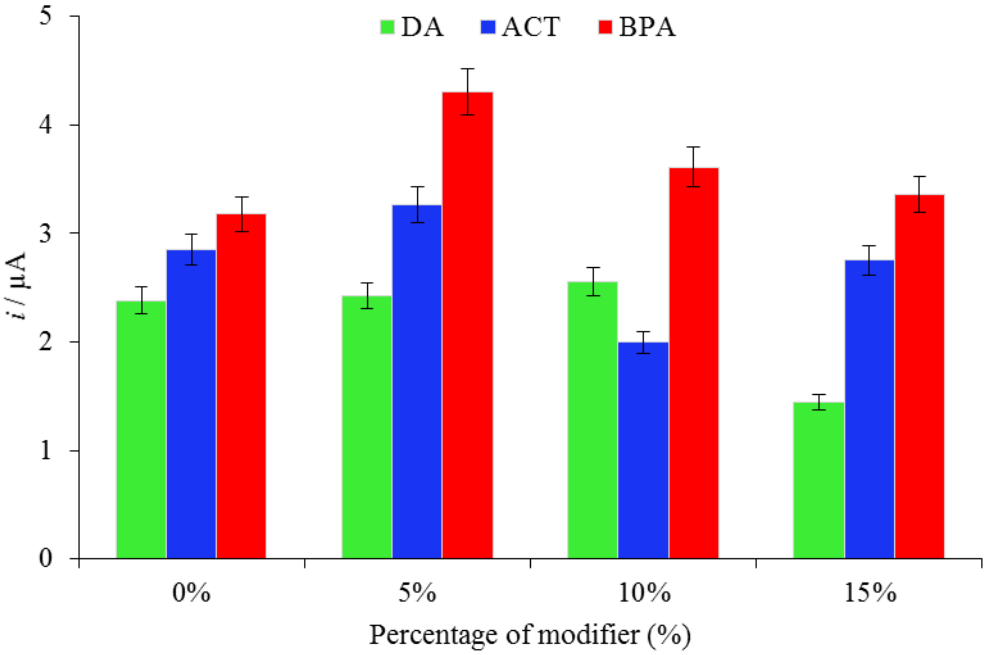

Figure 6. Graph of different composition ratios (% w/w) of Zn/Al-LDH-CP at modified MWCNT paste electrode.

3.4.2. Square wave voltammetry parameters

In SWV, some parameters applied such as frequency, step size, and pulse size may affect the electrode performance [47]. As shown in Fig. 7A, the effect of frequency was studied in the range of 90 Hz to 190 Hz. The peak current was increased up to 150 Hz and started to decrease at the frequency over 150 Hz. The range of pulse size from 10 to 60 mV was evaluated. As shown in Fig. 7B, the step size was measured between 2 mV until 8 mV and the highest peak current has been exhibited by step size 5 mV. The pulse size was measured between 10 mV until 60 mV (Fig. 7C). The peak current was increased with increasing of pulse size from 10 to 40 mV and further increasing of pulse size caused

the peak current to decrease. Thus, the optimum parameters used in this study were at frequency 150 Hz, step size 5 mV, and pulse size 40 mV.

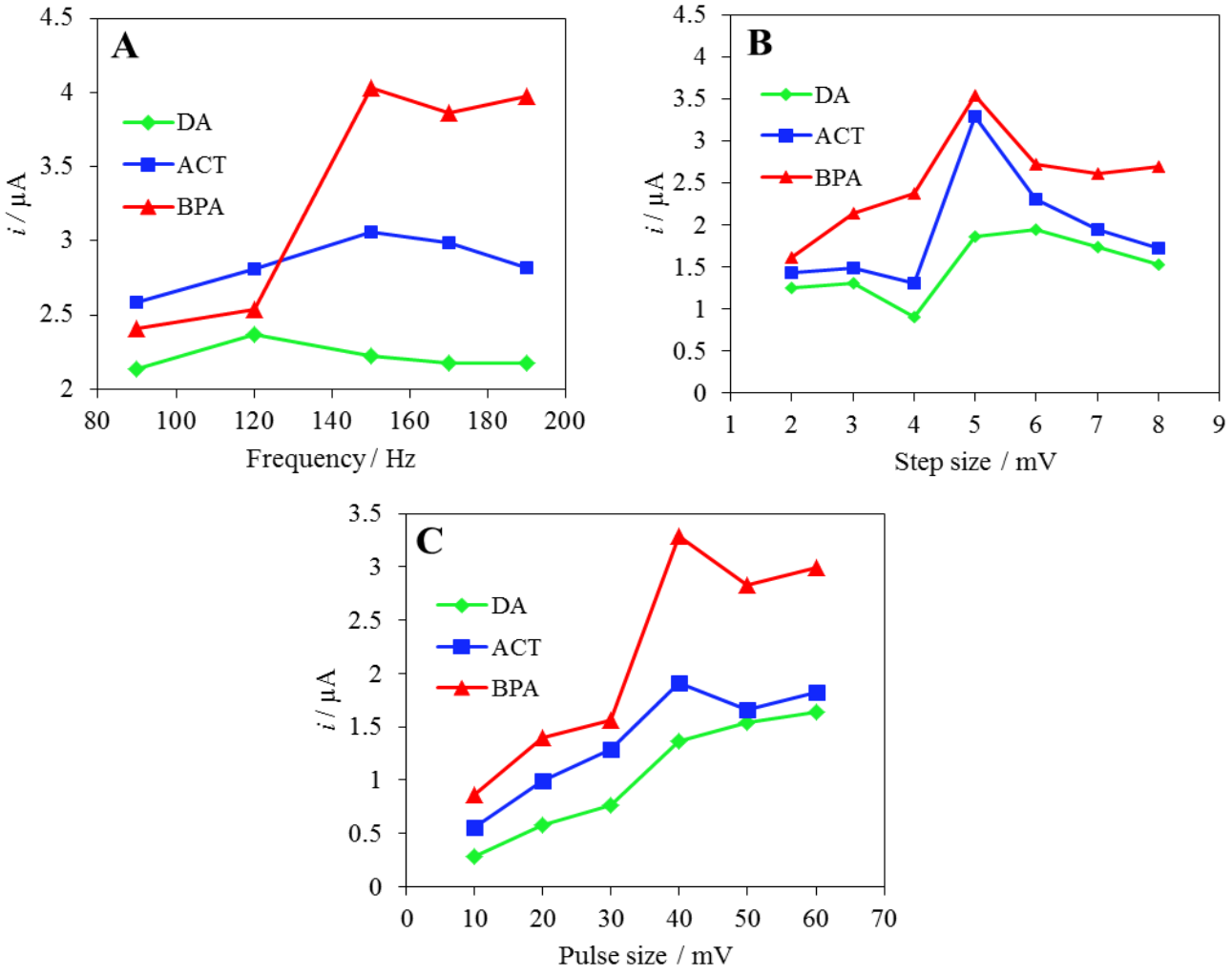

Figure 7. Effects of the SWV parameters (A) frequency, (B) step size, and (C) pulse size on current response. Solution: 1×10^{-4} M DA, ACT and BPA mixture.

3.4.3. Effects of solution pH

The effect of pH on the electrochemical response of 1.0×10^{-4} M DA, ACT, and BPA solution was studied over the pH ranges of 6.0 to 7.4. Fig. 8A (line a) shows that the peak current of DA increased with raising the solution pH until it reaches 7.0, and decreased at pH 7.4. The peak current of ACT in Fig. 8B (line a) initially decreased, and reached a better peak current at pH 7.0, then starts to diminish at higher pH. Whereas as shown in Fig. 8C (line a), the peak current of BPA was fluctuated and recorded a highest peak current at pH 7.0. Therefore, the pH value of 7.0, which show better resolution and near to biological pH value was selected for the subsequent experiments [48].

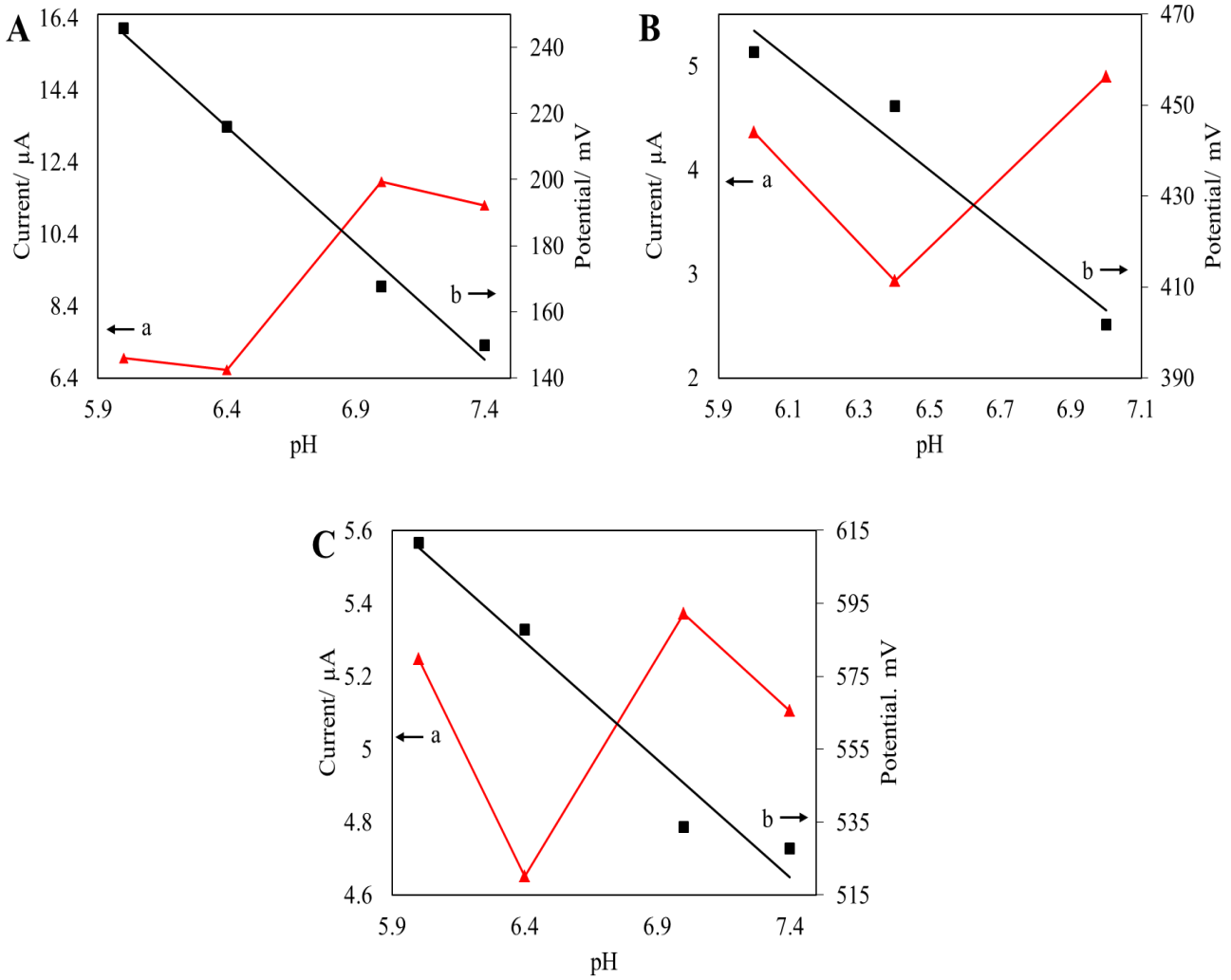

Figure 8. Graphs of current response (line a) and peak potential (line b) on varying pH value of (A) DA, (B) ACT, and (C) BPA solution.

Moreover, it can be seen in Fig. A (line b), Fig. B (line b) and Fig. C (line b), the peak potential decreased with increasing the pH value. This phenomenon also can be seen clearly from Fig. 9 as increasing of pH caused negatively shifting of the peak potential. The relationship can be expressed as E (mV) = -70.34 pH + 666.1 (R^2 = 0.9900) for DA, E (mV) = -61.50 pH + 835.4 (R^2 = 0.9517), and E (mV) = -64.62 pH + 998.1 (R^2 = 0.9565). The slopes obtained from the equations were close to the Nernst value (59.01 mV pH^{-1}) suggesting a balance number of protons and electrons in the electrochemical process [49]. Scheme 1 illustrates the probable electrochemical mechanism of DA, ACT and BPA at the Zn/Al-LDH-CP/MWCNTs paste electrodes. In the solution, DA is oxidized to dopamine-*o*-quinone, ACT is oxidized to *N*-acetyl-*p*-quinoneimine, and BPA is oxidized to 2,2-bis (4-phenylquinone) propane.

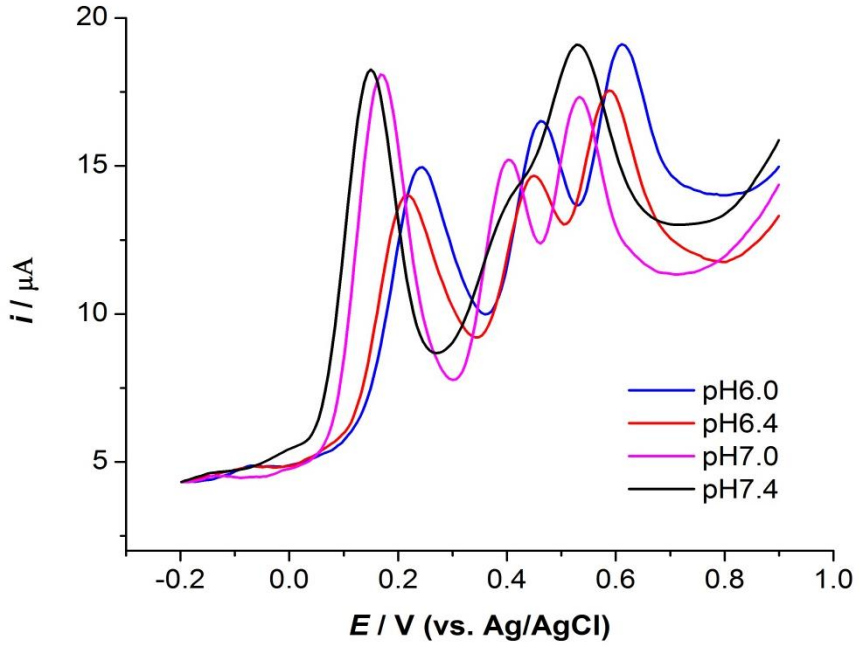

Figure 9. Square wave voltammograms of effect of pH value on the current response and peak potential of 1×10^{-4} M DA, ACT and BPA solution.

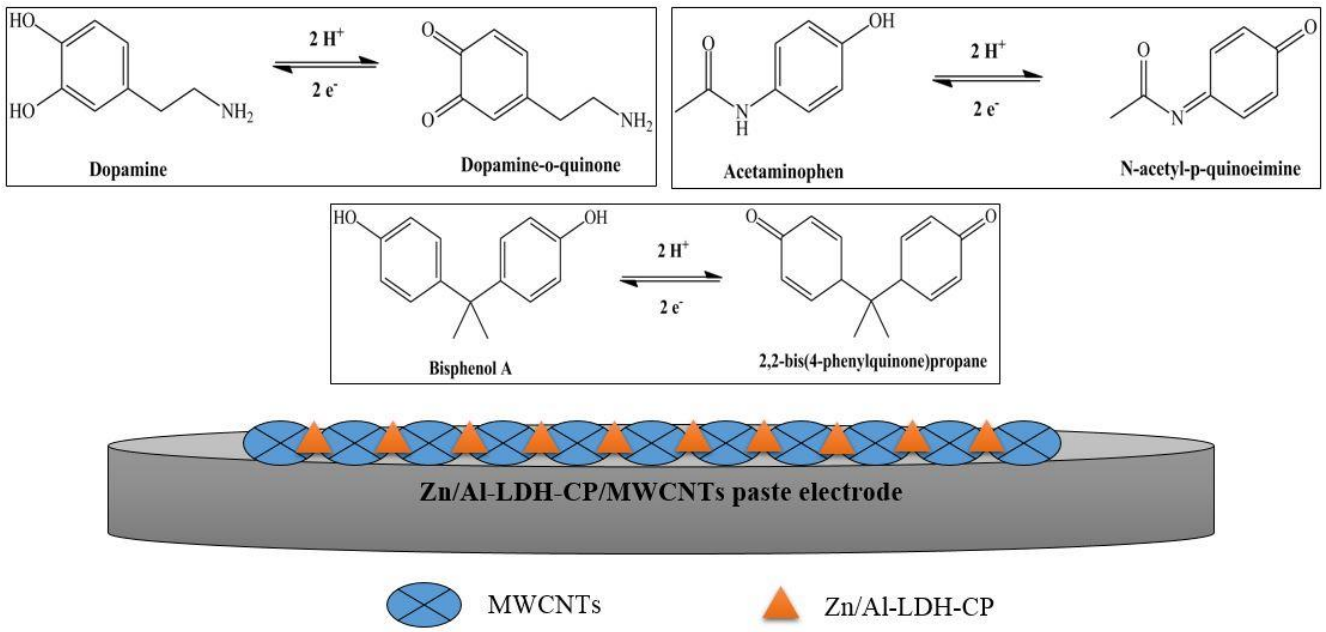

Scheme 1. Probable electrochemical mechanism of ACT, DA, and BPA at the Zn/Al-LDH-CP/MWCNTs paste electrode.

3.4.4. Scan rate effect

The effect of scan rate (70-350 mVs^{-1}) on the anodic peak current (I_{pa}) and the cathodic peak current (I_{pc}) of DA, ACT, and BPA at the surface of Zn/Al-LDH-CP/MWCNTs paste electrode was studied in 1.0 × 10^{-3} M DA, ACT, and BPA, respectively. Fig. 10A, 10B, and 10C depicts the increasing of the peak current of each analyte with increasing of scan rate.

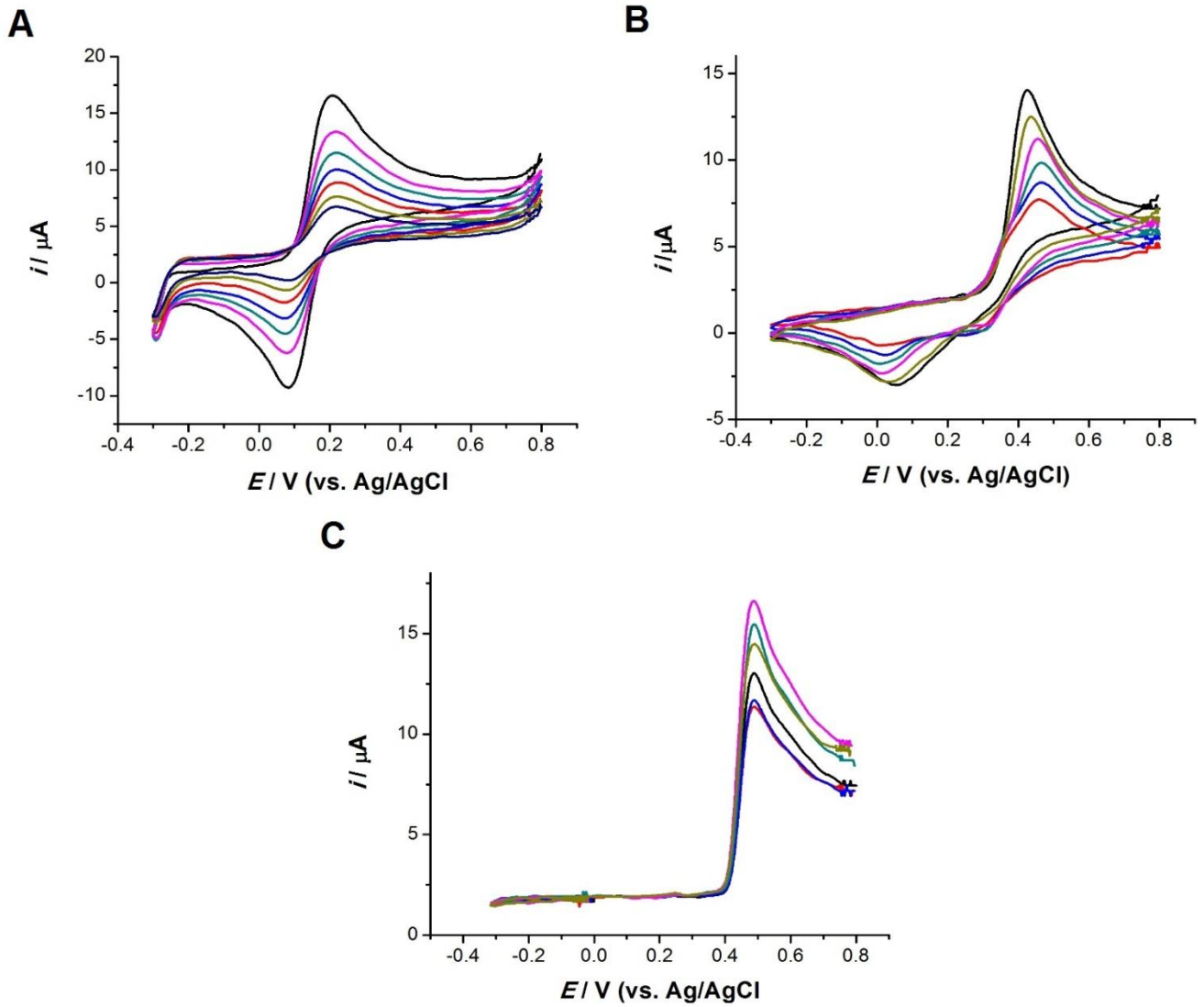

Figure 10. Cyclic voltammogram of Zn/Al-LDH-CP/MWCNT paste electrode with the different scan rates in 1 × 10^{-3} M of (A) DA, (B) ACT and (C) BPA.

Furthermore, it can be seen clearly in Fig. 11A, 11B, and 11C, the linear regression equations for DA: I_{pa} = 0.0275v + 1.184 (R = 0.9737) and I_{pc} = -0.031v + 0.4831 (R = 0.9657), for ACT: I_{pa} = 0.0302v + 2.827 (R = 0.9975) and I_{pc} = -0.0142v – 1.995 (R = 0.9854), and for BPA: I_{pa} = 0.019v + 1.170 (R = 0.9869). The results revealed that the reactions of DA, ACT, and BPA at the surface of the Zn/Al-LDH-CP/MWCNTs paste electrode were controlled by adsorption process [50]. Fig. 11D, 11E, and 11F illustrated that the log of peak current varies linearly with the log of scan rate by a slope value

of 0.98 for DA, 0.65 for ACT and 0.97 for BPA. These slopes are close to the theoretical value of 1.0, which further confirmed the adsorption controlled process owned by DA, ACT, and BPA at the surface of Zn/Al-LDH-CP/MWCNTs paste electrode [51].

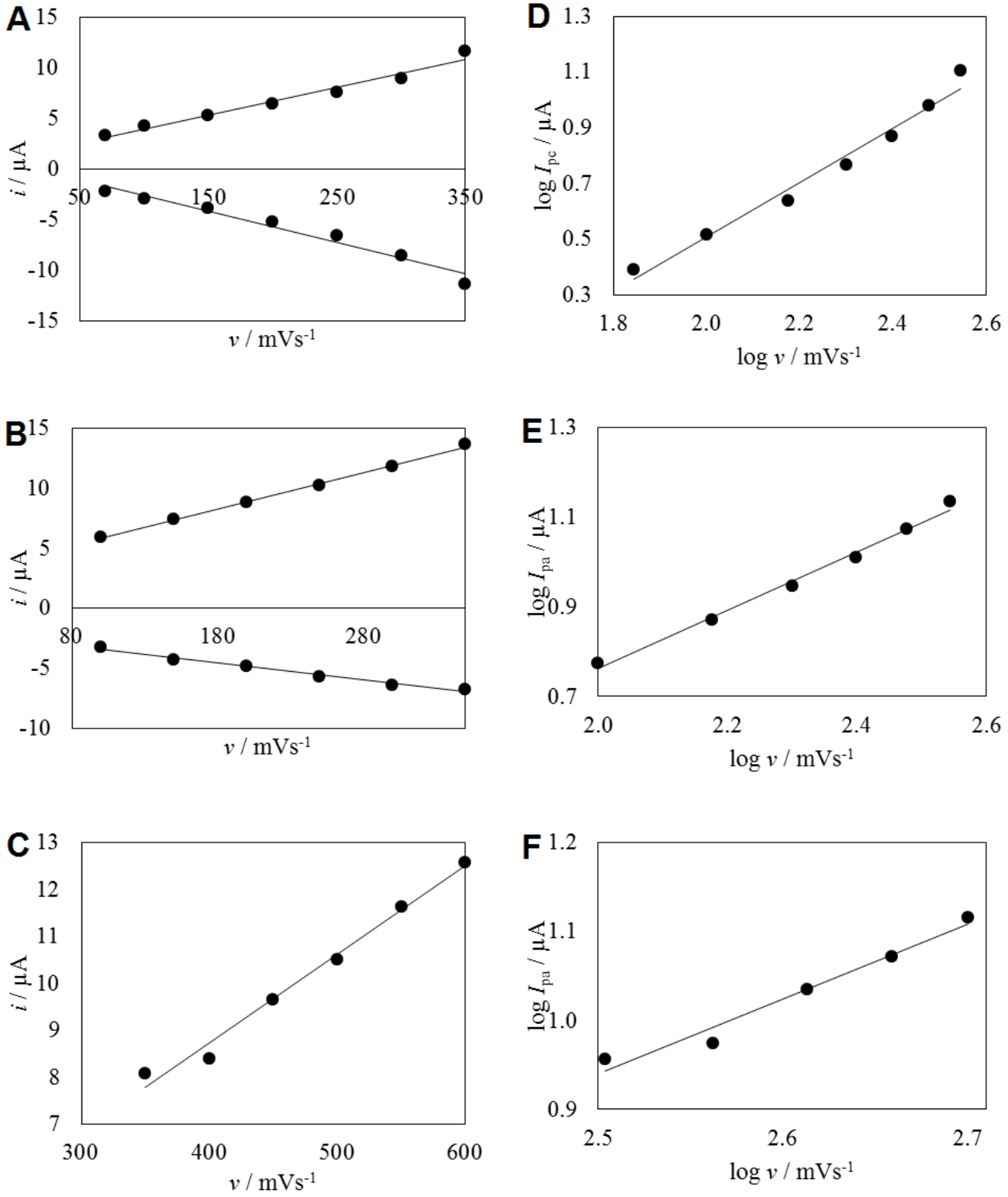

Figure 11. The graph of peak current versus scan rate for (A) DA, (B) ACT, and (C) BPA, and the graph of log peak current versus log scan rate for (D) DA, (E) ACT, and (F) BPA.

3.5. Chronocoulometry studies

Chronocoulometry studies were performed to investigate the effective electrochemical surface area, *A*, of MWCNTs and Zn/Al-LDH-CP/MWCNTs paste electrodes in 4.0 × 10^{-3} M $K_4Fe(CN)_6$ as a model complex. The *A* was calculated based on Anson equation:

$$Q(t) = \frac{2nFAcD^{\frac{1}{2}}t^{\frac{1}{2}}}{\pi^{\frac{1}{2}}} + Q_{dl} + Q_{ads}$$

Where *Q* (t) is a charge, *n* in a number of electron transfer, *F* is Faraday constant (96485 C mol^{-1}), *c* is a substrate concentration, *D* is diffusion coefficient of $K_4Fe(CN)_6$ and *t* is time. Q_{dl} is double layer charge which could be eliminated by background subtraction, and Q_{ads} is Faradaic charge Based on the slopes of the plots of *Q* vs. $t^{1/2}$ (Fig. 12A), the effective electrochemical surface area calculated for MWCNTs and Zn/Al-LDH-CP/MWCNTs paste electrode were 0.028 cm^2 and 0.063 cm^2, respectively. The increased of effective surface area might be resulted from the modification of MWCNTs paste electrode by Zn/Al-LDH-CP, which positively contributed to the increasing of the adsorption site and the current response of the electrode towards DA, ACT and BPA. The experiments were further carried out on the Zn/Al-LDH-CP/MWCNTs paste electrode in 1.0 × 10^{-4} M DA, ACT, and BPA solution. A plot of charge (*Q*) against the square root of time ($t^{1/2}$) (Fig.12B) was obtained after background subtraction and exhibited a slightly linear relationship. Hence, *D* for DA, ACT, and BPA were calculated to be 3.23 × 10^{-3} cm^2 s^{-1}, 4.37 × 10^{-4} cm^2 s^{-1}, and 3.51 × 10^{-4} cm^2 s^{-1}, respectively. According to the Cottrell equation, $Q_{ads} = nFA\Gamma_s$, the adsorption capacity, Γ_s, for DA, ACT, and BPA can be obtained as 3.39 x 10^{-9} mol cm^{-2}, 8.75 x 10^{-10} mol cm^{-2}, and 5.94 x 10^{-10} mol cm^{-2}, respectively.

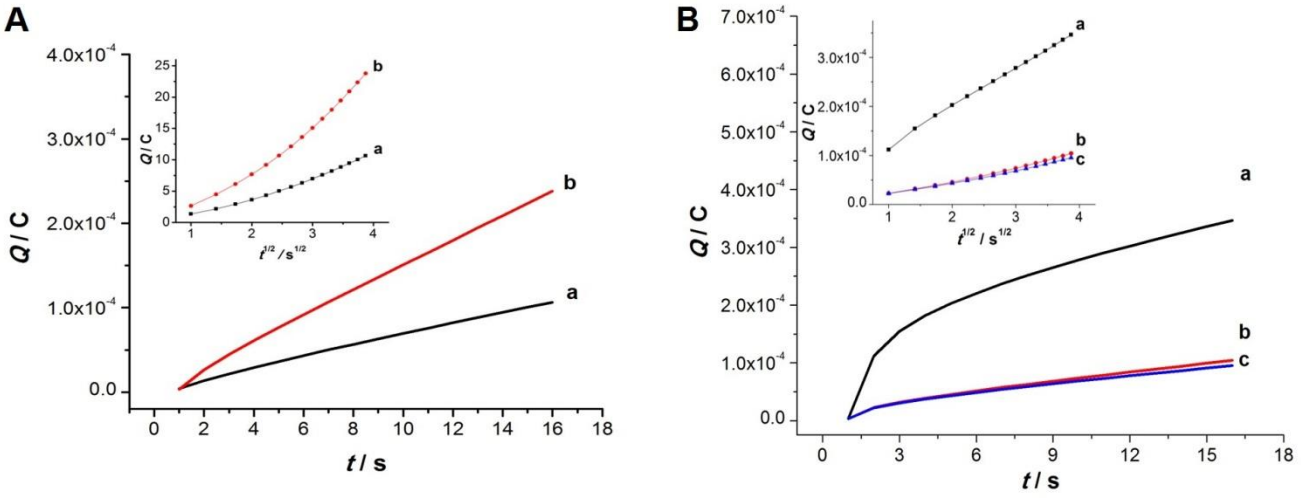

Figure 12. (A) Chronocoulograms of (a) MWCNT paste electrode, and (b) Zn/Al-LDH-CP/MWCNT paste electrode in 1.0 × 10^{-4} M $K_4Fe(CN)_6$, (B) Chronocoulograms of Zn/Al-LDH-CP/MWCNT paste electrode in 1 × 10^{-4} M (a) DA, (b) ACT, and (c) BPA solution. Scanning potential -0.3 – 2.0 V.

3.6. Simultaneous determination of DA, ACT, and BPA

The successive determination of DA, ACT, and BPA were performed using SWV at the Zn/Al-LDH-CP/MWCNTs paste electrode. As shown in Fig. 13, the linear relationship exhibited were in the range of 7.0×10^{-6} – 5.0×10^{-4} M ($R^2 = 0.9954$) for DA, 3.0×10^{-5} – 5.0×10^{-4} M ($R^2 = 0.9982$) for ACT, and 3.0×10^{-6} – 5.0×10^{-4} M ($R^2 = 0.9967$) for BPA. While their detection limit were 1.7×10^{-7} M, 1.8×10^{-7} M, and 1.4×10^{-7} M, respectively. Inset figure shows a logarithm graph of current versus analytes concentration for DA, ACT, and BPA. The relationship can be expressed as I/μA = 1.213 log [DA]/M + 12.49 ($R^2 = 0.9954$), I/μA = 1.856 log [ACT]/M + 19.51 ($R^2 = 0.9982$), and I/μA = 0.6689 log [BPA]/M + 8.752 ($R^2 = 0.9967$). These results were compared favorably with several reported studies as shown in Table 1.

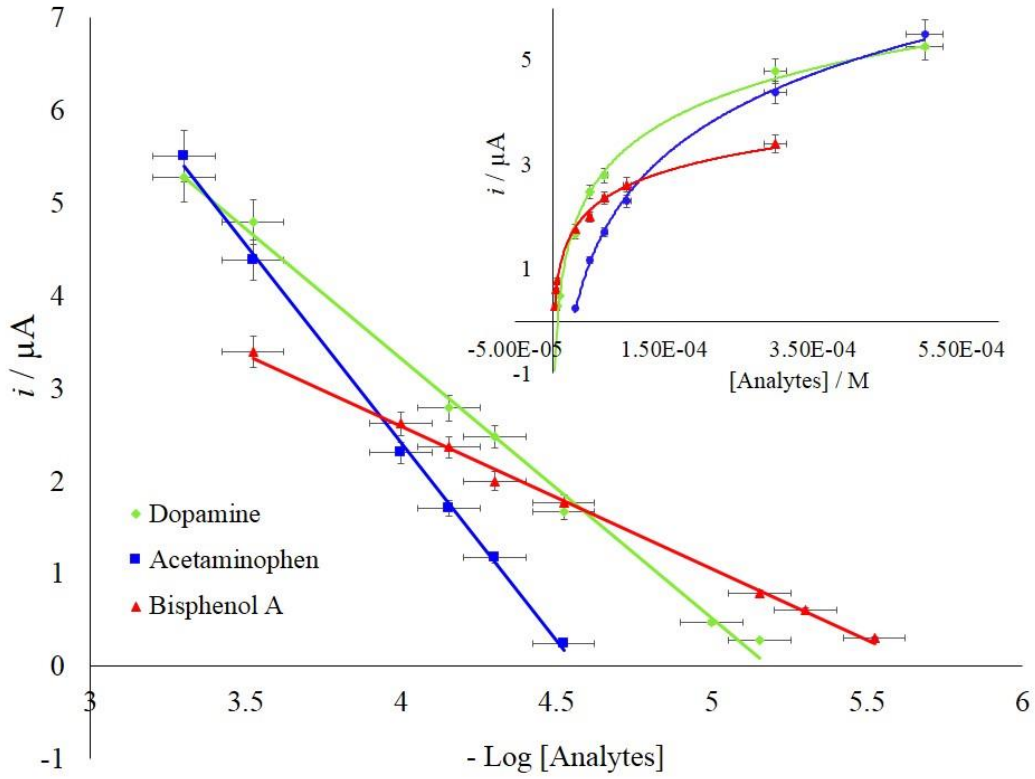

Figure 13. Calibration plots of various concentrations of DA, ACT, and BPA. (Inset: Graph peak current versus analytes concentration).

Table 1. Comparison between the current work and some reported sensors for the individual and simultaneous determination of the DA, ACT, and BPA.

Type of determination	Analyte	Electrode	LWR[a] (μM)	DL[b] (μM)	Ref.
Individual	DA	Ni-Al LDH/Carbon ionic liquid electrode	$1.0 \times 10^{-5} – 1.1 \times 10^{-3}$	5.0×10^{-6}	[36]
	DA	Ni-Al LDH/Graphene hybrid/GCE	Red: $5.0 \times 10^{-7} – 1.2 \times 10^{-4}$ Ox: $8.0 \times 10^{-5} – 4.0 \times 10^{-4}$	Red: 2.0×10^{-7} Ox: 9.6×10^{-6}	[35]
	ACT	Mg-Al LDH/NHNPs/MWCNTs/GCE	$2.0 \times 10^{-8} – 4.0 \times 10^{-5}$	5.0×10^{-9}	[37]
	ACT	Ni-Al LDH/Hexacyanoferrate/GCE	$3.0 \times 10^{-6} – 1.5 \times 10^{-3}$	8.0×10^{-7}	[52]
	ACT	ZLH-*L*-phenylalanate/MWCNTs paste electrode	$7.0 \times 10^{-7} – 1.0 \times 10^{-4}$	8.3×10^{-8}	[38]
	BPA	Mg-Al-CO_3 LDH/GCE	$1.0 \times 10^{-8} – 1.0 \times 10^{-6}$	5.0×10^{-9}	[40]
	BPA	Zn-Al ionic liquid-LDH/GCE	$2.0 \times 10^{-8} – 3.0 \times 10^{-6}$	4.6×10^{-9}	[41]
	BPA	Exfoliated Ni_2Al-LDH/Nanosheets	$2.0 \times 10^{-8} – 1.5 \times 10^{-6}$	6.8×10^{-9}	[39]
Simultaneous	DA	Porous gold nanosheets/GCE	$2.0 \times 10^{-6} – 3.0 \times 10^{-4}$	2.8×10^{-8}	[53]
	ACT		$3.0 \times 10^{-6} – 3.2 \times 10^{-4}$	2.3×10^{-8}	
	DA	MWCNT/GNS/GCE	$2.0 \times 10^{-6} – 2.0 \times 10^{-4}$	3.5×10^{-8}	[54]
	ACT		$2.0 \times 10^{-6} – 2.4 \times 10^{-4}$	2.3×10^{-8}	
	DA	Au/ZnO/N-doped grapheme/GCE	$2.0 \times 10^{-6} – 1.8 \times 10^{-4}$	4.0×10^{-7}	[55]
	ACT		$5.0 \times 10^{-6} – 3.1 \times 10^{-3}$	8.0×10^{-7}	
	DA	MWCNT/BPVCM/GCE	$5.0 \times 10^{-6} – 1.0 \times 10^{-3}$	2.3×10^{-6}	[56]
	ACT		$5.0 \times 10^{-6} – 1.0 \times 10^{-3}$	3.5×10^{-6}	
	DA	Zn/Al-LDH-CP/MWCNT/CPE	$7.0 \times 10^{-6} – 5.0 \times 10^{-4}$	1.7×10^{-7}	This work
	ACT		$3.0 \times 10^{-5} – 5.0 \times 10^{-4}$	1.8×10^{-7}	
	BPA		$3.0 \times 10^{-6} – 5.0 \times 10^{-4}$	1.4×10^{-7}	

[a] LWR – Linear working range.

[b] DL – Detection limit.

3.7. Reproducibility and repeatability

SWV measurements were used to study the reproducibility of the electrode by using two different electrodes which prepared under optimized conditions. The relative standard deviation (RSD) was determined as 4.76 %, 6.76 %, and 2.25 % for DA, ACT, and BPA respectively. Then, five measurements of a Zn/Al-LDH-CP/MWCNTs paste electrode were performed and the RSD obtained was 4.64 % for DA, 4.50 % for ACT, and 3.52 % for BPA.

3.8. Interferences studies

The interference from some organic compounds such as ascorbic acid, sodium salicylate, glucose, sucrose, glutamic acid, and captopril was studied. The results indicated that 10 and 25 fold

excess of those organic compounds do not interfere with the simultaneous determination of DA, ACT, and BPA with signal deviations less than 20% (Fig. 14). This clearly proved that the Zn/Al-LDH-CP/MWCNTs paste electrode had an excellent anti-interference ability.

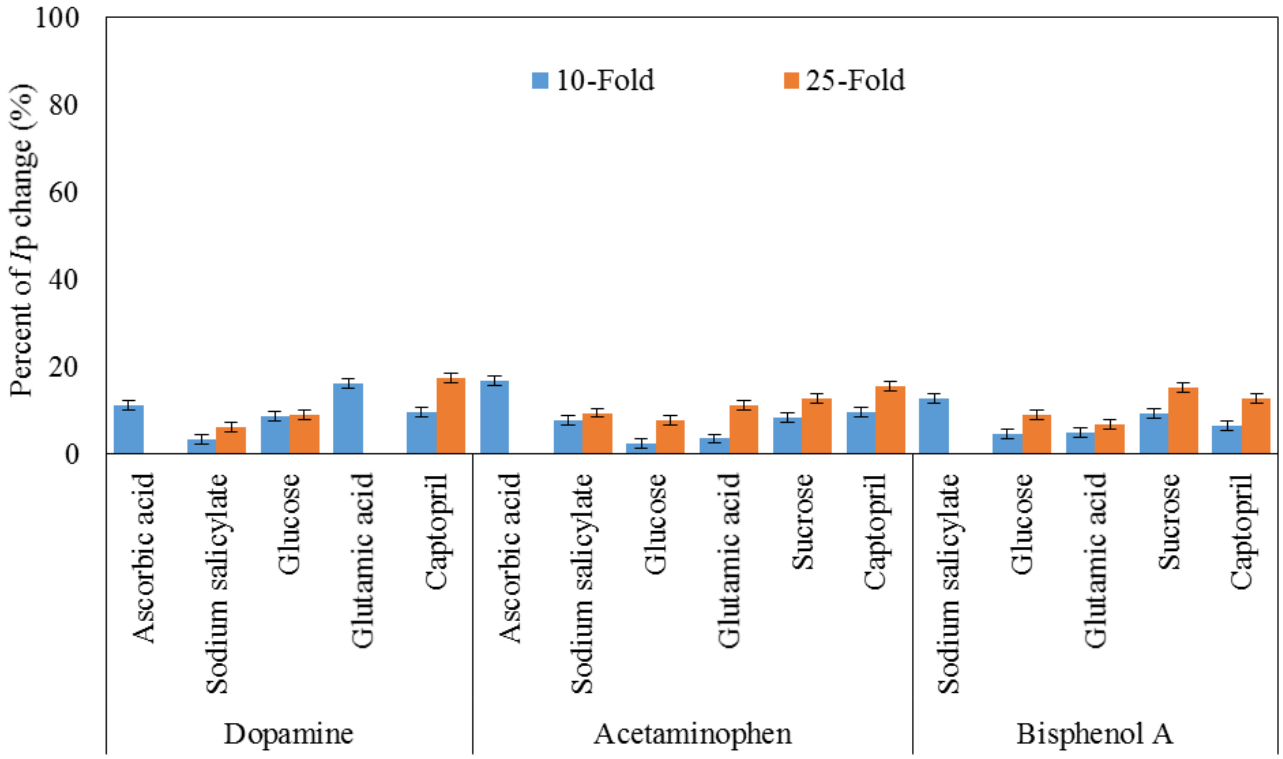

Figure 14. The effect of interferences in determination of DA, ACT, and BPA at Zn/Al-LDH-CP/MWCNT paste electrode.

3.9. Analytical application of Zn/Al-LDH-CP/MWCNTs paste electrode

The applicability of the Zn/Al-LDH-CP/MWCNTs paste electrode was tested for the determination of DA in urine samples, ACT in pharmaceutical tablets, and BPA in baby teether. Recoveries were calculated based on the standard addition method. As shown in Table 2, the recoveries were between 92.33 % and 109.7%. Therefore, the electrode could be successfully practiced for the determination of DA, ACT, and BPA in real samples.

Table 2. Recoveries of ACT, DA, and BPA in various samples.

Sample	Detected (μM)	Added (μM)		Found (μM)	Recovery (%)
Urine 1	N.D. [a]	DA	2.80×10^{-5}	2.77×10^{-5}	99.1
		ACT	2.80×10^{-5}	2.59×10^{-5}	92.3
		BPA	2.80×10^{-5}	2.79×10^{-5}	99.8

Urine 2	N.D.	DA	2.80×10^{-5}	2.94×10^{-5}	105.0
		ACT	2.80×10^{-5}	2.87×10^{-5}	102.5
		BPA	2.80×10^{-5}	3.00×10^{-5}	107.0
Paracil 500 mg	2.31	DA	2.80×10^{-5}	3.07×10^{-5}	109.7
		ACT	2.80×10^{-5}	5.37×10^{-5}	105.0
		BPA	2.80×10^{-5}	2.81×10^{-5}	100.3
Panadol 120mg	3.19	DA	2.80×10^{-5}	3.00×10^{-5}	107.0
		ACT	2.80×10^{-5}	6.26×10^{-5}	104.6
		BPA	2.80×10^{-5}	2.93×10^{-5}	104.8
Baby teether	2.67	DA	2.80×10^{-5}	2.86×10^{-5}	102.1
		ACT	2.80×10^{-5}	2.70×10^{-5}	96.4
		BPA	2.80×10^{-5}	2.97×10^{-5}	96.7

[a] ND – Not detected.

4. CONCLUSIONS

The use of Zn/Al-LDH-CP as a modifier in the simultaneous determination of DA, ACT, and BPA was successfully demonstrated. The Zn/Al-LDH-CP/MWCNTs paste electrode shows increasing in electron transfer rate and a better conductivity through CV and EIS studies. Based on chronocoulometry studies, the modified electrode exhibits a large effective electrochemical surface area and high adsorption capacity. At optimal condition, the electrode shows a wide linear range of DA, ACT, and BPA concentration with a detection limit of 1.7×10^{-7} M, 1.8×10^{-7} M and 1.4×10^{-7} M, respectively.

ACKNOWLEDGEMENTS
The authors acknowledge the support from the Ministry of Education Malaysia and Universiti Pendidikan Sultan Idris (grant numbers 2017-0075-101-02).

References

1. C.A. Frye, E. Bo, G. Calamandrei, L. Calza, F. Desso-Fulgheri, M. Fernandez, L. Fusani, O. Kah, M. Kajta, Y. Le Page, H.B. Patosaul, A. Venerosi, A.K. Wojtowicz and G.C. Panzica, *J. Neuroendocrinol.*, 24 (2011) 144.
2. J.R. Rochester, *Reprod. Toxicol.*, 42 (2013) 132.
3. K.H. Cox, J.D. Gatewood, C. Howeth and E.F. Rissman, *Horm. Behav.*, 58 (2010) 754.
4. K. Nakamura, K. Itoh, H. Dai, L. Han, X. Wang, S. Kato, T. Sugimoto and S. Fushiki, *Brain Dev.*, 34 (2012) 57.
5. A. Mirzahosseini, T. Palla, G. Orgovan, G. Toth and B. Noszal, *J. Pharmaceut. Biomed.*, 158 (2018) 346.
6. A. Westbrook and M. Frank, *Curr. Opin. Behav. Sci.*, 22 (2018) 28.
7. A.A. Macdonald, K.N. Seergobin, A.M. Owen, R. Tamjeedi, O. Monchi, H. Ganjavi and P.A. Macdonald, *PLoS One*, 8 (2013) e74044.
8. O. Howes, R. Mccutcheon and J. Stone, *J. Psychopharmacol.*, 29 (2015) 97.
9. G.B. Steventon, M.T.E. Heafield, R.H. Waring, A.C. Williams, S. Sturman and M. Green,

Xenobiotica, 20 (2015) 117.
10. C.J. Locke, S.A. Fox, G.A. Caldwell and K.A. Caldwell, *Neurosci. Lett.,* 439 (2008) 129.
11. E. Yoon, A. Babar, M. Choudhary, M. Kutner and N. Pyrsopoulos, *J. Clin. Transl. Hepatol.,* 4 (2016) 131.
12. S. Shiffman, D.R. Battista, J.P. Kelly, M.K. Malone, R.B. Weinstein and D.W. Kaufman, *J. Am. Pharm. Assoc.,* 58 (2018) 499.
13. M.D. Martin Black, *Annu. Rev. Med.,* 35 (1984) 577.
14. C. Bunchorntavakul and K.R. Reddy, *Clin. Liver Dis.,* 17 (2013) 587.
15. Y.M. Issa, M.E.M. Hassouna and A.G. Zayed, *J. Liq. Chromatogr. Relat. Technol.,* 35 (2012) 2148.
16. S.A. Haeri, *J. Chromatogr. B,* 1028 (2016) 186.
17. M.A. Mallah, S.T.H. Sherazi, M.I. Bhanger, S.A. Mahesar and M.A. Bajeer, *Spectrochim. Acta A,* 141 (2015) 64.
18. Y. Li, P. Lu, J. Cheng, X. Zhu, W. Guo, L. Liu, Q. Wang, C. He and S. Liu, *Talanta,* 187 (2018) 207.
19. M. Amjadi, J.L. Manzoori and T. Hallaj, *J. Lumin.,* 158 (2015) 160.
20. W. Gao, L. Qi, Z. Liu, S. Majeed, S.A. Kitte and G. Xu, *Sens. Actuators B:Chem.,* 238 (2017) 468.
21. S. Erdemir and O. Kocyigit, *Sens. Actuators B:Chem.,* 221 (2015) 900.
22. Q. Kong, Y. Wang, L. Zhang, S. Ge and J. Yu, *Sens. Actuators B:Chem.,* 243 (2017) 130.
23. M.S. Ahmad, I.M. Isa, N. Hashim, M.I. Saidin, S.M. Si, R. Zainul, A. Ulianas and S. Mukdasai, *Int. J. Electrochem. Sc.,* 14 (2019) 9080.
24. A.J.S. Ahammad, J.J. Lee and M.A. Rahman, *Sensors,* 9 (2009) 2289.
25. M. Pumera, A. Merkoci and S. Alegret, *Sens. Actuators B:Chem.,* 113 (2006) 617.
26. M. Pumera, S. Samuel, I. Ichinose and J. Tang, *Sens. Actuators B:Chem.,* 123 (2007) 1195.
27. G.A. Rivas, M.D. Rubianes, M.C. Rodr, N.F. Ferreyra, G.L. Luque, M.L. Pedano, S.A. Miscoria and C. Parrado, *Talanta,* 74 (2007) 291.
28. L. Agui, P.Y. Sedeno and J.M. Pingarron, *Anal. Chim. Acta.,* 622 (2008) 11.
29. F. Cavani, F. Trifiro and A. Vaccari, *Catal. Today,* 11 (1991) 173.
30. L. Fernández, C. Borrás, J. Mostany and B. Scharifker, Layered double hydroxides for electrochemical sensing application, in: R.J. Tremont (Ed.), Recent Advances in Electrochemical Research, Transworld Research Network, Kerala, 2012.
31. S.N.M. Sharif, N. Hashim, I.M. Isa, S.A. Bakar, M.I. Saidin, M.S. Ahmad, M. Mamat and M.Z. Hussein, *Mater. Chem. Phy*., 251 (2020) 123076.
32. D. Tonelli, E. Scavetta and M. Giorgetti, *Anal. Bioanal. Chem.,* 405 (2013) 603.
33. X.S. Dan, L. Yang, W.Z. Yang, S.G. Li and Y.R. Qin, *Chin. J. Anal. Chem.,* 43 (2015) 1648.
34. N. Baig and M. Sajid, *Trends Environ. Anal. Chem.,* 16 (2017) 1.
35. M. Li, J.E. Zhu, L. Zhang, X. Chen, H. Zhang, F. Zhang, S. Xu and D.G. Evans, *Nanoscale,* 3 (2011) 4240.
36. Z. Zhu, L. Qu, Y. Guo, Y. Zeng, W. Sun and X. Huang, *Sens. Actuators B:Chem.,* 151 (2010) 146.
37. A. Babaei, M. Afrasiabi and G. Azimi, *Anal. Methods,* 7 (2015) 2469.
38. M.S. Ahmad, I. Isa, N. Hashim, S.M. Si and M.I. Saidin, *J. Solid State Electrochem.,* 22 (2018) 2691.
39. T. Zhan, Y. Song, Z. Tan and W. Hou, *Sens. Actuators B:Chem.,* 238 (2017) 962.
40. H. Yin, L. Cui, S. Ai, H. Fan and L. Zhu, *Electrochim. Acta,* 55 (2010) 603.
41. T. Zhan, Y. Song, X. Li and W. Hou, *Mater. Sci. Eng. C,* 64 (2016) 354.
42. F. Ye, C. Feng, J. Jiang and S. Han, *Electrochim. Acta,* 182 (2015) 935.
43. B. Baś, A. Bugajna, M. Jakubowska, W. Reczyński and A. Smalec, *Electrochim. Acta,* 99 (2013) 190.

44. G. Bolat, Y.T. Yaman and S. Abaci, *Sens. Actuators B:Chem.,* 255 (2018) 140.
45. G.G.C. Arizaga, K.G. Satyanarayana and F. Wypych, *Solid State Ion.*, 178 (2007) 1143.
46. A. Sharma, J.K. Bhattarai, S.S. Nigudkar, S.G. Pistorio, A.V Demchenko, and K.J. Stine, *J. Electroanal. Chem.,* 782 (2016) 174.
47. J.G. Osteryoung and R.A. Osteryoung, *Anal. Chem.,* 57 (1985) 101A.
48. A. Babaei, A. Dehdashti & M. Afrasiabi, *Int. J. Electrochem.*, 2011 (2011) 452629
49. R. Zainul, N.A. Azis, I.M. Isa, N. Hashim, M.S. Ahmad, M.I. Saidin and S. Mukdasai, *Sensors*, 19 (2019) 941.
50. N. Elgrishi, K.J. Rountree, B.D. McCarthy, E.S. Rountree, T.T. Eisenhart and J.L. Dempsey, *J. Chem. Educ.*, 95 (2018) 197.
51. E. Laviron, L. Roullier and C. Degrand, *J. Electroanal. Chem.*, 112 (1980) 11.
52. K.A Zeynali and R. Amini, *Electroanalysis*, 29 (2017) 635.
53. Q.L. Zhang, J.X. Feng, A.J. Wang, J. Wei, Z.Y. Lv and J.J. Feng, *Microchim. Acta,* 182 (2015) 589.
54. S. Zhang, P. He, G. Zhang, W. Lei and H. He, *Anal. Sci.*, 31 (2015) 657.
55. X. Chen, G. Zhang, L. Shi, S. Pan, W. Liu and H. Pan, *Mater. Sci. Eng. C,* 65 (2016) 80-89.
56. R. Liu, X. Zeng, J. Liu, J. Luo, Y. Zheng and X. Liu, *Microchim. Acta*, 183 (2016) 1543.